Near-infrared modulation by means of GeTe/SOI based metamaterial

E. Petronijevic,[1,*] G. Leahu,[1] V. Di Meo,[2,3] A. Crescitelli,[3] P. Dardano,[3] G. Coppola,[3] E. Esposito,[3] I. Rendina,[3] M. Miritello,[4] M. G. Grimaldi,[4,5] V. Torrisi,[6] G. Compagnini,[6] C. Sibilia[1]

[1]Department S.B.A.I., Sapienza Università di Roma, Via A. Scarpa 14 I-00161, Rome, Italy
[2]Department D.I.M.E.S, University of Calabria, Via P. Bucci, Rende, Italy
[3]Institute for Microelectronics and Microsystems – CNR Napoli, Via P. Castellino 111, Naples, Italy
[4]Institute for Microelectronics and Microsystems – CNR Catania, Via S. Sofia 64, Catania, Italy
[5]Department of Physics and Astronomy, Università di Catania, Via S. Sofia 64, Catania, Italy
[6]BRIT (Bio-nanotech Research and Innovation Tower), Università di Catania, via S. Sofia 89, Catania, Italy
*Corresponding author: emilija.petronijevic@uniroma1.it

Received XX Month XXXX; revised XX Month, XXXX; accepted XX Month XXXX; posted XX Month XXXX (Doc. ID XXXXX); published XX Month XXXX

Nowadays nanophotonics still lacks components for modulation that can be easily implementable in the existing silicon-on-insulator (SOI) technology. Chalcogenide phase change materials (PCM) are promising candidates for the tuning in the near-infrared: at the nanoscale, thin layers can provide enough contrast to control optical response of a nanostructure. Moreover, all-dielectric metamaterials allow for the resonant behavior without having ohmic losses in the telecom range. Here, a novel hybridization of SOI-based metamaterial with PCM GeTe is experimentally investigated. A metamaterial based on Si nanorods, covered by a thin layer of GeTe is designed and fabricated. Switching of GeTe from amorphous to crystalline leads to a rather high resonance-governed reflection contrast at 1.55 μm. Additional confocal Raman imaging is done to differentiate the crystallized zones of the metamaterials' unit cell. The findings are in good agreement with numerical analysis and show good perspectives of all-dielectric tunable near-infrared nanophotonics.

http://dx.doi.org/10.1364/OL.99.099999

Over the past decades, the advances in nanotechnology have enabled realization of metamaterials, specially engineered nanoresonators organized in the periodic sub-wavelength arrays [1]. Metamaterials are usually based on plasmonic resonances that can efficiently tailor the light propagation at the nanoscale, thus providing nano-analogues of conventional optical components [2,3]. However, once realized, the metamaterial has a fixed optical response, while future photonic circuitry needs active, tunable, fast and reconfigurable components. This issue has led to progress in the research of hybridization of metamaterials with phase change materials (PCM). Most of PCM have phases that dramatically differ in optical properties, so that a thin PCM layer combined with a metamaterial can provide high amplitude or phase change of the optical field. Specifically, PCM such as chalcogenide glasses usually possess at least two solid phases that are stable at room temperature: amorphous and crystalline (defined by covalent and resonant bonding, respectively). Heat stimuli can provide a non-volatile switching between these phases over large number of cycles, which is the reason behind their conventional use in rewritable storage [4]. More recently, PCM-functionalized nanodevices have been proposed for low-dimensional optoelectronic platforms [5], on-chip photonic memory elements [6,7] and numerous nanoscale photonic devices based on PCM-metamaterial approach have found applications in optical switching [8], lensing [9,10], beam steering [11], tunable absorbers [12-14] etc. In the near-infrared, chalcogenide PCM such as GeTe, $Ge_2Sb_2Te_5$ (GST), $Ge_3Sb_2Te_6$ and $Ge_8Sb_2Te_{11}$ are of great interest due to low optical losses [15]; in [16] GeTe has been used for modulation of surface plasmon polaritons in a plasmonic metamaterial. On the other hand, the losses of the metamaterial structure can be significantly lowered by using high refractive index dielectric resonators instead of the plasmonic ones [17,18]; e.g. Si-based metamaterials [19,20] have been already proven to provide sharp resonances in the telecom range, while having straightforward fabrication and implementation in the conventional Si-based technology. In our previous work we have numerically proposed a combination of the all-dielectric metamaterials with thin layers of PCM GST [21] and GeTe [22] for the transmission switching in the near-infrared.

Here we investigate an all-dielectric metamaterial based on Si nanorods (NRs) and combined with GeTe. The nanostructure is

fabricated by patterning a conventional Silicon on insulator (SOI) wafer to provide a collective dipole-like resonance in the near-infrared, and then covering it by a thin GeTe layer. Switching from the amorphous (*GeTe-am*) to the crystalline *(GeTe-cr)* state provides a modulation in the optical response, leading to a notable difference at 1.55 μm. In order to characterize this difference, we perform a reflection scan of the metasurfaces in both states and at different wavelengths; we measure the contrast ratio of ~5 at 1.55 μm, and no contrast at 1.31 μm. Moreover, we perform confocal Raman imaging to differentiate the crystallized zones of the sample. As these experimental results are in good agreement with numerical predictions, we believe that the SOI-PCM metamaterial approach can find applications in the near-infrared, chip-scale, tunable photonics.

A 2D periodical array of NRs was fabricated by Electron Beam Lithography and Reactive Ion Etching from a SOI wafer with the buried oxide thickness t_{SiO2}=3 μm, and the upper Si thickness of t=220 nm. The patterned area of (100x100) μm^2 was chosen to ensure the collective NR response [19], and a scanning electron microscopy (SEM) image of the obtained sample of good quality is shown in Fig. 1(a). The NR length L=840 nm, width W=300 nm, and the periodicity p=950 nm were chosen to provide a dipole-like resonance in the range around 1.5 μm. Subsequently, a 30 nm of stoichiometric GeTe-am layer was deposited on the metamaterial surface by RF sputtering [23]. In Fig. 1(b) we show the sketch of the nanostructure's unit cell.

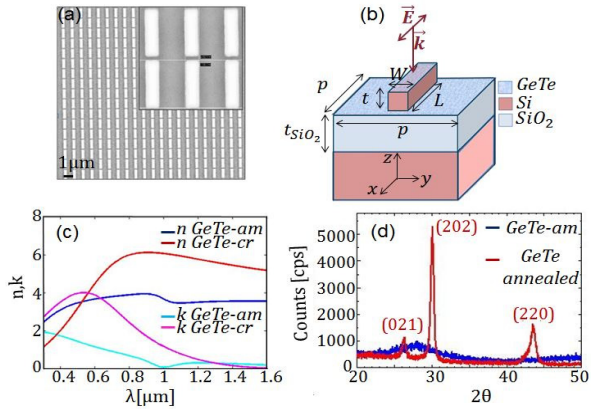

Fig. 1. (a) Top view SEM image Si NR metamaterial fabricated from SOI wafer. (b) Sketch of the unit cell with the geometric parameters and the thin layer of GeTe. (c) Ellipsometry characterization of the amorphous and crystalline reference GeTe films. (d) XRD spectra of the reference GeTe film before and after the annealing.

The stoichiometry and the optical constants of *GeTe-am* and *GeTe-cr* were measured on a flat sample constituted of a 100 nm thick GeTe deposited on c-Si. The stoichiometry of GeTe has been verified by Rutherford Back-Scattering Spectrometry. Ellipsometric measurements [24] were performed to determine the optical constants of the amorphous and crystalline phases, using a crystallization temperature of 200°C, Fig. 1(c). The crystallization of the reference sample was also verified by X-Ray diffraction (XRD) measurements performed with a Bruker-AXSD5005 diffractometer by using a Cu Kα radiation with an incidence angle of 0.5° and the detection angle 2θ varied between 20° and 50°. The XRD spectra before and after the thermal treatment are reported in Fig. 1(d): the appearance of peaks for 2θ of 26°, 30° and 43° after the annealing demonstrates the crystallization of the film. The XRD peaks correspond to respectively the (021), (202) and (220) crystalline planes of GeTe crystalline phase [JCPDS 00-047-1079].

We further experimentally characterize the metamaterial behavior for the two states of GeTe by means of the position scan along the metasurface, and the corresponding reflection at 1.31 μm and 1.55 μm. First measurements were done with the metamaterial covered by *GeTe-am*. Then, the whole structure was slowly heated above the crystallization temperature (i.e. to 200°C, as for the reference sample), and the reflection scan was repeated. The experimental set-up is shown in Fig. 2(a). Firstly, the NR metamaterial needs to be individualized in the big, unpatterned area of the wafer, which is covered by GeTe as well. A Quartz Tungsten Halogen (QTH) lamp and microscope are used to position the patterned part of the sample, observed by color CCD camera. Then, QTH is replaced by a Ge photo-diode to measure the reflection and the sample is shined with laser light polarized in x-direction, under normal incidence, with the spot size of ~15 μm. The sample is put on the movable stage which allows for the position scan with the scan step of 2 μm, where one measures the light reflection from the unpatterned and the metamaterial zones of the sample. The results in Fig. 2(b) show the reflection dependence on the laser position. In the unpatterned zones (|laser position|>50 μm), at both wavelengths the thin crystalline layer is highly reflective, as expected. Entering the metamaterial zone leads to the interplay between PCM properties and the NRs: the reflection is effectively lowered in all cases except for the *GeTe-am* at 1.55 μm. Moreover, as the laser position approaches the center of the metamaterial, this reflection increases; in the center, the contribution of the collective resonant response is the highest, thus leading to the noticeable reflection contrast between metamaterial covered by *GeTe-am* and *GeTe-cr* at 1.55 μm. The thermally induced phase change is the first step for the characterization of SOI-GeTe hybrid metamaterial approach; in the future, optical switching could provide fast, non-volatile and reconfigurable reflection switching, while the patterning of the whole structure after the GeTe deposition could lead to sharper resonances providing higher contrast [22].

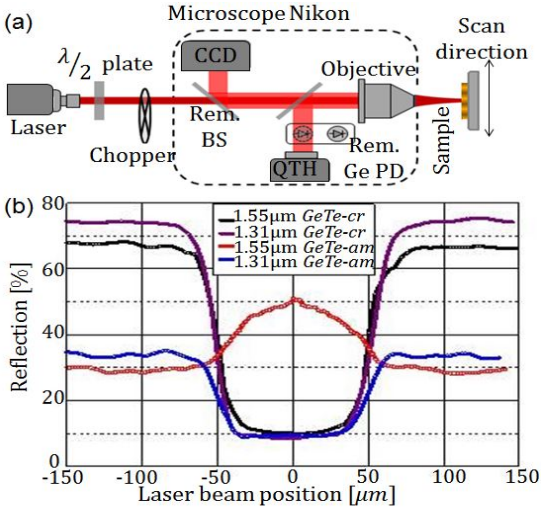

Fig. 2. (a) Experimental set-up for the measurement of the reflection from SOI-GeTe hybrid metamaterial versus laser beam position; two lasers at 1.31 μm and 1.55 μm were used to demonstrate the different behavior of the metasurface. (b) Reflection as the dependence on the laser position from the center of the metamaterial, for the two states. Inside the metamaterial, the reflection is low in all cases except for the *GeTe-am* at 1.55 μm.

In order to confirm the phase change of the thin GeTe layers on the patterned surface, we perform micro-Raman confocal miscroscopy at 632 nm, in reflection geometry. First, we monitor the Raman response of flat GeTe layers in the unpatterned zones of the structure, before, and after the heating. Raman spectra, reported in Fig. 3(a), for *GeTe-am* (red) and *GeTe-cr* (blue), are in good agreement with the literature [25]. In the range 50–200 cm^{-1} we can distinguish three bands, peaked respectively around 80 cm^{-1}, 120 cm^{-1} and 164 cm^{-1}. In the amorphous phase the third band appears more prominent with respect the crystalline phase where the second one is the more intense, moreover all the bands appear blue-shifted in the amorphous case with respect to the crystalline phase. Thus, by exciting the patterned surface we have recorded the Raman response from the SOI-GeTe hybrid metamaterial. The Raman maps of the signals at 118 cm^{-1} and 164 cm^{-1} have been reported in Fig. 3(b) and Fig. 3(c) respectively. It is evident that the Raman signals are strongly dependent on the position: in particular, on the top of the NRs the signal at 118 cm^{-1} is maximized, while it has its minimum in the zones between the NRs (Fig. 3(b)), where instead the maximum Raman signal at 164 cm^{-1} is maximized (Fig. 3(c)). It suggests the prevalence of the signal relative to crystalline GeTe on the top of the NRs, and of the one relative to amorphous between the NRs. Finally, Fig. 3(d) reports the false-color combination image, obtained by Witec Project 4.0 software, that combines the Raman maps of the signals at 118 cm^{-1} and at 164 cm^{-1}: the red region refers to the prevalence of the signal at 164 cm^{-1}, relative to amorphous GeTe, and the blue region refers to the prevalence of the signal at 118 cm^{-1}, relative to crystalline GeTe. Therefore, the structure of the GeTe film above the NRs and at the bottom is different: the amount of crystal at the bottom is definitely lower than that above the NRs. Such a behavior can be ascribed to the different stress suffered, during the phase change, by the film on the top or at the bottom of the NRs due to a different constraint of the surrounding materials. In fact, the strain due to the volume change during the transformation (amorphous molar volume 0.179 cm^3/g, crystal molar volume 0.165 cm^3/gr [26]), is likely to be released more efficiently on top of the NR, where there are no lateral constraints, giving rise to a higher crystallization rate. Previously, we designed metamaterials governed by the control of PCM only on the top of nanoresonator [21]; this shows great promise for the low-power, optically induced phase change, where only a small volume of GeTe must be switched in order to change the overall metamaterial response.

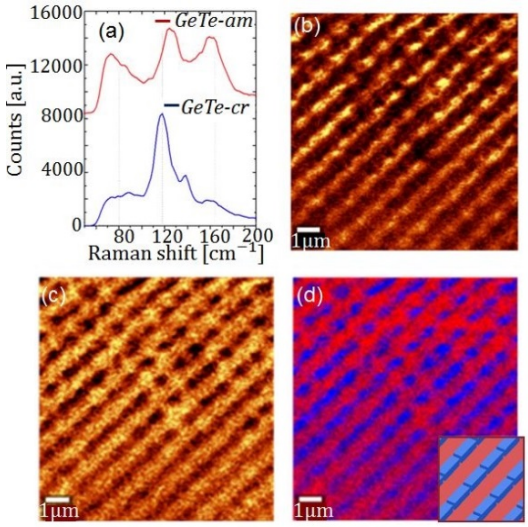

Fig. 3. (a) Raman spectra for the amorphous and crystalline flat layers of GeTe upon SOI, in the unpatterned part of the structure. The dotted lines indicate 80 cm^{-1}, 118 cm^{-1} and 164 cm^{-1}. (b) Raman map from the hybrid metamaterial of the signal at 118 cm^{-1} and (c) at 164 cm^{-1}. (d) False-color combination image of the Raman maps from the hybrid metamaterial of the signals at 164 cm^{-1} (red), and at 118 cm^{-1} (blue); inset: the metamaterial sketch.

In order to confirm the metamaterial-GeTe governed reflection contrast, we use the finite-difference time-domain (FDTD) solver by Lumerical [27]. We apply periodic boundary conditions in the metamaterial xy plane, while in the z-direction we apply perfectly matched layer (PML) conditions. The metamaterial is excited from the NR side by a plane wave, linearly polarized along the NR (x-direction), under normal incidence. In order to prevent numerical instabilities, we ensure that PML boundaries are at least half the maximum wavelength distant from the NR, and from the bottom of the SiO_2 layer. The Si NR with previous dimensions, placed on a SiO_2 substrate, provides a broad transmission dip, i.e. reflection peak in the near-infrared, as shown in Fig. 4(a); in the inset the z-component of the electric field is shown. The same NR, with 30nm *GeTe-am* on the top, has slightly blue-shifted resonance, and the reflection peak is lowered due to losses of GeTe. Changing the GeTe phase to crystalline produces a red-shift of the resonance and an increase of the reflectivity (the losses are lower, Fig. 1(c)). This strong red shift is due to notably higher refractive index of the crystalline state; this effect has been previously noted in more complicated all-dielectric metamaterials [24], and can lead to high optical contrast ratio between the resonance in the amorphous state and the off-resonant behavior in the crystalline state. Next, we investigate the influence of the structure with buried SiO_2 on the metamaterial optical properties, important for the implementation in reliable and conventional SOI technology. Figure 4(b) shows the metamaterial reflection dependence on the thickness t_{SiO2}, around the telecom wavelengths. First, without the deposited GeTe layer (Fig. 4(b)-left), after ~1 μm a broad dipole-like resonant behavior is noted with oscillations due to the interference in the SiO_2 layer [17,20]. Since the GeTe deposition was done after the patterning, we further include the thin *GeTe-am* layer on both NRs and the SiO_2 part of the substrate. The interference-governed behavior is still noted in Fig. 4(b)-middle, but PCM layers in this configuration lead to high red shift and

broadening of the resonances; for t_{SiO2}=3 μm the resonance comprises 1.55 μm. Then, the GeTe crystallization on the NR leads to even higher red shift (to short-wave infra-red), while at 1.55 μm there is a low reflection, Fig. 4(b)-right. Specifically, for t_{SiO2}=3 μm at 1.55 μm, GeTe-metamaterial reflection is lowered from ~56% to ~11% when GeTe changes from amorphous to crystalline, which is in good agreement with measurements (from ~50% to ~10%, Fig. 2(b)). Moreover, we numerically investigate *GeTe-am* to *GeTe-cr* evolution of the reflection response inside (GeTe-NRs) and outside (GeTe-SOI) of the metamaterial; we use the effective medium theory and Lorentz-Lorenz [28,29] fit to calculate complex refractive index dependence on the crystallization level. We define the contrast of the reflection between *GeTe-am* and partially crystallized *GeTe-part* as $CR=R_{GeTe\text{-}am}/R_{GeTe\text{-}part}$. In Fig. 4(c) for GeTe-SOI (unpatterned zones in Fig. 2(b)), at both wavelengths, as well as for GeTe-NRs at 1.31 μm, CR decreases with crystallization, and it is below 1, as expected for the highly reflective crystalline state. Instead, for GeTe-NRs at 1.55 μm, this contrast inverts, and reaches 5.2 for the complete crystallization, providing a route to high optical contrast between the resonance-governed states of the all-dielectric metamaterial-PCM structure. The crosses of the corresponding colors are the experimental CR values; their good agreement shows promise for the design and optimization of GeTe-hybridized all-dielectric metamaterials.

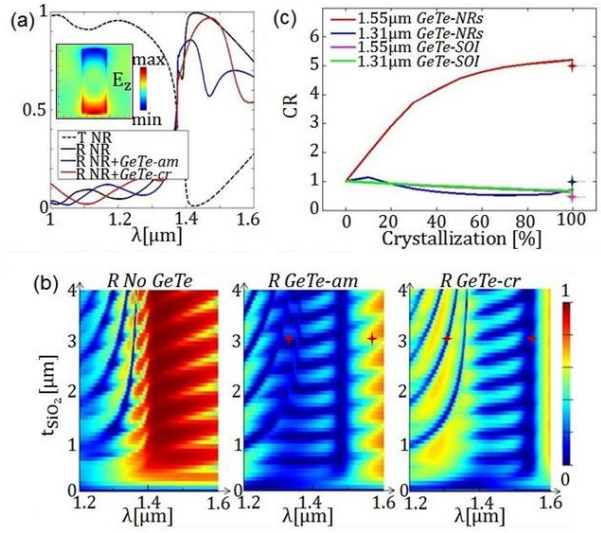

Fig. 4. (a) Optical response of the NR metamaterial with and without GeTe. Inset: z-component of the electric field at the dipole-like resonance. (b) Metamaterial reflection dependence on t_{SiO2}: left - without GeTe; middle - when the metamaterial is covered by *GeTe-am*; right - when GeTe on the top of the NRs is switched to *GeTe-cr*; red stars are the experimental points. (c) Reflection contrast defined as $CR=R_{GeTe\text{-}am}/R_{GeTe\text{-}part}$ inside (GeTe-NRs) and outside (GeTe-SOI) of the metamaterial at 1.31 μm and 1.55 μm.

In conclusion, we have proposed a near-infrared reflection switching in the SOI-based metamaterial, covered by PCM GeTe. GeTe shows high real refractive index change in the near-infrared, while having the low losses; this is of great interest for the tunable, all-dielectric nanophotonics, implementable in SOI chip-scaled technology. We characterize the reflection change from the metasurface when the amorphous GeTe on the top of the NR changes to crystalline. Furthermore, we use the confocal micro-Raman spectroscopy to characterize the GeTe state, and map the crystallized area. Finally, the position reflection scan out of and inside the metamaterial surface shows good agreement with numerical simulations. We believe that the all-dielectric, low-loss GeTe-SOI-based metamaterials could find future applications in tunable, non-volatile nanophotonic devices.

1. N. I. Zheludev and Y. S. Kivshar, Nat. Mater. 11, 917–924 (2012).
2. N. Yu and F. Capasso, Nat. Mater. 13(2), 139–150 (2014).
3. J. P. Balthasar Mueller, N. A. Rubin, R. C. Devlin, B. Groever, and F. Capasso, Phys. Rev. Lett. 118(11), 113901 (2017).
4. M. Wuttig, and N. Yamada, Nat. Mater. 6, 824-832 (2007).
5. P. Hosseini, C. D. Wright, and H. Bhaskaran, Nature 511 (7508), 206–211 (2014).
6. P. Hosseini, C. D. Wright, H. Bhaskaran, and W. H. P. Pernice, Adv. Mater. 26 (9), 1372–1377 (2014).
7. Z. Cheng, C. Ríos, W. H. P. Pernice, C. D. Wright, and H. Bhaskaran, Sci. Adv. 3(9), e1700160 (2017).
8. B. Gholipour, J. Zhang, K. F. MacDonald, D. W. Hewak, and N. I. Zheludev, Adv. Mater. 25(22), 3050–3054 (2013).
9. X. Yin, T. Steinle, L. Huang, T. Taubner, M. Wuttig, T. Zentgraf, and H. Giessen, Light Sci. Appl. 6(7), e17016 (2017).
10. Y. Chen, X. Li, Y. Sonnefraud, A. I. Fernández-Domínguez, X. Luo, M. Hong, and S. A. Maier, Sci. Rep. 5(1), 8660 (2015).
11. C. Ruiz de Galarreta, A. M. Alexeev, Y.-Y. Au, M. Lopez-Garcia, M. Klemm, M. Cryan, J. Bertolotti, and C. D. Wright, Adv. Funct. Mater. 28(10), 1704993 (2018).
12. A. Tittl, A.-K. U. Michel, M. Schäferling, X. Yin, B. Gholipour, L. Cui, M. Wuttig, T. Taubner, F. Neubrech, and H. Giessen, Adv. Mater. 27(31), 4597–4603 (2015).
13. T. Cao, C. W. Wei, R. E. Simpson, L. Zhang, and M. J. Cryan, Sci. Rep. 4(1), 3955 (2014).
14. S. G. Carrillo, A. M. Alexeev, Y. Au, and C. D. Wright, Opt. Express 26(20), 25567–25581 (2018).
15. A. - K. U. Michel, M. Wuttig, and T. Taubner, Adv. Optical Mater. 5, 1700261 (2017).
16. M. Jafari and M. Rais-Zadeh, Opt. Lett. 41(6), 1177-1180 (2016).
17. A. García-Etxarri, R. Gómez-Medina, L. S. Froufe-Pérez, C. López, L. Chantada, F. Scheffold, J. Aizpurua, M. Nieto-Vesperinas, and J. J. Sáenz, Opt. Express 19(6), 4815–4826 (2011).
18. J. van de Groep and A. Polman, Opt. Express 21(22), 26285–26302 (2013).
19. Y. Yang, I. I. Kravchenko, D. P. Briggs, and J. Valentine, "All-dielectric metasurface analogue of electromagnetically induced transparency," Nat. Commun. 5, 5753 (2014).
20. Y. Yang, W. Wang, A. Boulesbaa, I. I. Kravchenko, D. P. Briggs, A. Puretzky, D. Geohegan, and J. Valentine, Nano Lett. 15(11), 7388–7393 (2015).
21. E. Petronijevic and C. Sibilia, Opt. Express 24, 30411 (2016).
22. E. Petronijevic and Concita Sibilia, Proc. SPIE 10228, Nonlinear Optics and Applications X, 102280K (2017).
23. A.M. Mio, E. Carria, G. D'Arrigo, S. Gibilisco, M. Miritello, M. G. Grimaldi, and E. Rimini, J. Non-Cryst. Solids 357, 2197–2201 (2011).
24. P. Dardano, M. Gagliardi, I. Rendina, S. Cabrini, and V. Mocella, Light: Science & Applications 1.12 (2012).
25. K. S. Andrikopoulos, S. N. Yannopoulos, G. A. Voyiatzis, A. V. Kolobov, M. Ribes, and J. Tominaga, J. Phys. Condens. Matter 18, 965–979 (2006).
26. T. Nonakaa, G. Ohbayashia, Y. Toriumib, Y. Morib, H. Hashimoto, Thin Sol. Films 370, 258-261 (2000).
27. Lumerical Solutions, Inc. http://www.lumerical.com/tcad-products/fdtd/
28. N. V. Voshchinnikov, G. Videen, and T. Henning, Appl. Opt. 46(19), 4065–4072 (2007).
29. TY. G. Chen, T. S. Kao, B. Ng, X. Li, X. G. Luo, B. Luk'yanchuk, S. A. Maier, M. H. Hong, Opt. Express 21(11), 13691-13698 (2013).